

## SPT-CL J0205–5829: A $z = 1.32$ EVOLVED MASSIVE GALAXY CLUSTER IN THE SOUTH POLE TELESCOPE SUNYAEV–ZEL'DOVICH EFFECT SURVEY

B. STALDER<sup>1</sup>, J. RUEL<sup>2</sup>, R. ŠUHADA<sup>3</sup>, M. BRODWIN<sup>4</sup>, K. A. AIRD<sup>5</sup>, K. ANDERSSON<sup>3,6</sup>, R. ARMSTRONG<sup>7</sup>, M. L. N. ASHBY<sup>1</sup>, M. BAUTZ<sup>6</sup>, M. BAYLISS<sup>2</sup>, G. BAZIN<sup>3,8</sup>, B. A. BENSON<sup>9,10</sup>, L. E. BLEEM<sup>9,11</sup>, J. E. CARLSTROM<sup>9,10,11,12,13</sup>, C. L. CHANG<sup>9,10,13</sup>, H. M. CHO<sup>14</sup>, A. CLOCCHIATTI<sup>15</sup>, T. M. CRAWFORD<sup>9,12</sup>, A. T. CRITES<sup>9,12</sup>, T. DE HAAN<sup>16</sup>, S. DESAI<sup>3,8</sup>, M. A. DOBBS<sup>16</sup>, J. P. DUDLEY<sup>16</sup>, R. J. FOLEY<sup>1</sup>, W. R. FORMAN<sup>1</sup>, E. M. GEORGE<sup>17</sup>, D. GETTINGS<sup>18</sup>, M. D. GLADDERS<sup>9,12</sup>, A. H. GONZALEZ<sup>18</sup>, N. W. HALVERSON<sup>19</sup>, N. L. HARRINGTON<sup>17</sup>, F. W. HIGH<sup>9,12</sup>, G. P. HOLDER<sup>16</sup>, W. L. HOLZAPFEL<sup>17</sup>, S. HOOVER<sup>9,10</sup>, J. D. HRUBES<sup>5</sup>, C. JONES<sup>1</sup>, M. JOY<sup>20</sup>, R. KEISLER<sup>9,11</sup>, L. KNOX<sup>21</sup>, A. T. LEE<sup>17,22</sup>, E. M. LEITCH<sup>9,12</sup>, J. LIU<sup>3,8</sup>, M. LUEKER<sup>17,23</sup>, D. LUONG-VAN<sup>5</sup>, A. MANTZ<sup>9</sup>, D. P. MARRONE<sup>24</sup>, M. McDONALD<sup>6</sup>, J. J. McMAHON<sup>9,10,25</sup>, J. MEHL<sup>9,12</sup>, S. S. MEYER<sup>9,11,10,12</sup>, L. MOCANU<sup>9,12</sup>, J. J. MOHR<sup>3,8,26</sup>, T. E. MONTRY<sup>27</sup>, S. S. MURRAY<sup>1</sup>, T. NATOLI<sup>9,11</sup>, D. NURGALIEV<sup>2</sup>, S. PADIN<sup>9,12,23</sup>, T. PLAGGE<sup>9,12</sup>, C. PRYKE<sup>28</sup>, C. L. REICHARDT<sup>17</sup>, A. REST<sup>29</sup>, J. E. RUHL<sup>27</sup>, B. R. SALIWANCHIK<sup>27</sup>, A. SARO<sup>3</sup>, J. T. SAYRE<sup>27</sup>, K. K. SCHAFFER<sup>9,10,30</sup>, L. SHAW<sup>16,31</sup>, E. SHIROKOFF<sup>17,23</sup>, J. SONG<sup>25</sup>, H. G. SPIELER<sup>22</sup>, S. A. STANFORD<sup>21,32</sup>, Z. STANISZEWSKI<sup>27</sup>, A. A. STARK<sup>1</sup>, K. STORY<sup>9,11</sup>, C. W. STUBBS<sup>1,2</sup>, A. VAN ENGELEN<sup>16</sup>, K. VANDERLINDE<sup>16</sup>, J. D. VIEIRA<sup>9,11,23</sup>, A. VIKHЛИNIN<sup>1</sup>, R. WILLIAMSON<sup>9,12</sup>, O. ZAHN<sup>17,33</sup>, AND A. ZENTENO<sup>3,8</sup>

<sup>1</sup> Harvard-Smithsonian Center for Astrophysics, 60 Garden Street, Cambridge, MA 02138, USA; bstalder@cfa.harvard.edu

<sup>2</sup> Department of Physics, Harvard University, 17 Oxford Street, Cambridge, MA 02138, USA

<sup>3</sup> Department of Physics, Ludwig-Maximilians-Universität, Scheinerstr. 1, D-81679 München, Germany

<sup>4</sup> Department of Physics, University of Missouri, 5110 Rockhill Road, Kansas City, MO 64110, USA

<sup>5</sup> University of Chicago, 5640 South Ellis Avenue, Chicago, IL 60637, USA

<sup>6</sup> MIT Kavli Institute for Astrophysics and Space Research, Massachusetts Institute of Technology, 77 Massachusetts Avenue, Cambridge, MA 02139, USA

<sup>7</sup> National Center for Supercomputing Applications, University of Illinois, 1205 West Clark Street, Urbana, IL 61801, USA

<sup>8</sup> Excellence Cluster Universe, Boltzmannstr. 2, D-85748 Garching, Germany

<sup>9</sup> Kavli Institute for Cosmological Physics, University of Chicago, 5640 South Ellis Avenue, Chicago, IL 60637, USA

<sup>10</sup> Enrico Fermi Institute, University of Chicago, 5640 South Ellis Avenue, Chicago, IL 60637, USA

<sup>11</sup> Department of Physics, University of Chicago, 5640 South Ellis Avenue, Chicago, IL 60637, USA

<sup>12</sup> Department of Astronomy and Astrophysics, University of Chicago, 5640 South Ellis Avenue, Chicago, IL 60637, USA

<sup>13</sup> Argonne National Laboratory, 9700 S. Cass Avenue, Argonne, IL 60439, USA

<sup>14</sup> NIST Quantum Devices Group, 325 Broadway Mailcode 817.03, Boulder, CO 80305, USA

<sup>15</sup> Departamento de Astronomía y Astrofísica, Pontificia Universidad Católica, Chile

<sup>16</sup> Department of Physics, McGill University, 3600 Rue University, Montreal, Quebec H3A 2T8, Canada

<sup>17</sup> Department of Physics, University of California, Berkeley, CA 94720, USA

<sup>18</sup> Department of Astronomy, University of Florida, Gainesville, FL 32611, USA

<sup>19</sup> Department of Astrophysical and Planetary Sciences and Department of Physics, University of Colorado, Boulder, CO 80309, USA

<sup>20</sup> Department of Space Science, VP62, NASA Marshall Space Flight Center, Huntsville, AL 35812, USA

<sup>21</sup> Department of Physics, University of California, One Shields Avenue, Davis, CA 95616, USA

<sup>22</sup> Physics Division, Lawrence Berkeley National Laboratory, Berkeley, CA 94720, USA

<sup>23</sup> California Institute of Technology, 1200 E. California Blvd., Pasadena, CA 91125, USA

<sup>24</sup> Steward Observatory, University of Arizona, 933 North Cherry Avenue, Tucson, AZ 85721, USA

<sup>25</sup> Department of Physics, University of Michigan, 450 Church Street, Ann Arbor, MI, 48109, USA

<sup>26</sup> Max-Planck-Institut für extraterrestrische Physik, Giessenbachstr., D-85748 Garching, Germany

<sup>27</sup> Physics Department, Center for Education and Research in Cosmology and Astrophysics, Case Western Reserve University, Cleveland, OH 44106, USA

<sup>28</sup> Physics Department, University of Minnesota, 116 Church Street S.E., Minneapolis, MN 55455, USA

<sup>29</sup> Space Telescope Science Institute, 3700 San Martin Dr., Baltimore, MD 21218, USA

<sup>30</sup> Liberal Arts Department, School of the Art Institute of Chicago, 112 S Michigan Avenue, Chicago, IL 60603, USA

<sup>31</sup> Department of Physics, Yale University, P.O. Box 208210, New Haven, CT 06520-8120, USA

<sup>32</sup> Institute of Geophysics and Planetary Physics, Lawrence Livermore National Laboratory, Livermore, CA 94551, USA

<sup>33</sup> Berkeley Center for Cosmological Physics, Department of Physics, University of California, and Lawrence Berkeley National Labs, Berkeley, CA 94720, USA

*Received 2012 May 29; accepted 2012 November 4; published 2013 January 14*

## ABSTRACT

The galaxy cluster SPT-CL J0205–5829 currently has the highest spectroscopically confirmed redshift,  $z = 1.322$ , in the South Pole Telescope Sunyaev–Zel'dovich (SPT-SZ) survey. *XMM-Newton* observations measure a core-excluded temperature of  $T_X = 8.7^{+1.0}_{-0.8}$  keV producing a mass estimate that is consistent with the Sunyaev–Zel'dovich-derived mass. The combined SZ and X-ray mass estimate of  $M_{500} = (4.8 \pm 0.8) \times 10^{14} h_{70}^{-1} M_\odot$  makes it the most massive known SZ-selected galaxy cluster at  $z > 1.2$  and the second most massive at  $z > 1$ . Using optical and infrared observations, we find that the brightest galaxies in SPT-CL J0205–5829 are already well evolved by the time the universe was  $< 5$  Gyr old, with stellar population ages  $\gtrsim 3$  Gyr, and low rates of star formation ( $< 0.5 M_\odot \text{ yr}^{-1}$ ). We find that, despite the high redshift and mass, the existence of SPT-CL J0205–5829 is not surprising given a flat  $\Lambda\text{CDM}$  cosmology with Gaussian initial perturbations. The a priori chance of finding a cluster of similar rarity (or rarer) in a survey the size of the  $2500 \text{ deg}^2$  SPT-SZ survey is 69%.

**Key words:** early universe – galaxies: clusters: individual (SPT-CL J0205–5829) – galaxies: evolution – galaxies: formation – large-scale structure of universe

**Online-only material:** color figure

## 1. INTRODUCTION

The South Pole Telescope (SPT; Carlstrom et al. 2011) has recently completed a survey designed to discover all massive galaxy clusters within a  $2500 \text{ deg}^2$  region of the southern sky. High-redshift galaxy clusters are valuable as probes of the initial conditions of the universe, particularly the distribution of matter at early epochs. Since galaxy clusters are the most massive collapsed systems, their abundance is sensitive to the properties of the early universe, including Gaussianity around the peak of the matter density field (e.g., Lucchin & Matarrese 1988; Colafrancesco et al. 1989; Mortonson & Hu 2010) and the nature of inflationary models. In addition to cosmology, the constituent galaxies of these clusters, which have essentially co-evolving star formation histories (SFHs), are useful for studying galaxy formation and evolution.

The SPT-SZ survey finds clusters via the Sunyaev–Zel'dovich (SZ; Sunyaev & Zel'dovich 1972) effect. The vast majority of baryonic mass of a galaxy cluster is in the form of diffuse, ionized gas, known as the intracluster medium (ICM), unassociated with any particular galaxy. Photons from the cosmic microwave background (CMB) are Compton scattered by the free electrons in this ionized gas. The scattered photons gain energy on average leading to a spectral distortion of the observed CMB known as the thermal SZ effect. The surface brightness of the SZ effect is independent of the distance to the cluster because the SZ effect depends solely on the line-of-sight integral of thermal pressure of the ionized gas. Therefore the total SZ flux is a measure of the total thermal energy in the gas, which is tightly correlated to the cluster mass. This makes SZ surveys an efficient means for finding high-mass clusters at all redshifts (e.g., Carlstrom et al. 2002).

Observations of fine scale CMB anisotropy with the SPT, Planck Satellite (Planck Collaboration et al. 2011), and Atacama Cosmology Telescope (ACT; Marriage et al. 2011) have recently been used to detect massive clusters in large surveys of the sky. The progress of the cluster survey by SPT is reported by Staniszewski et al. (2009), Vanderlinde et al. (2010), Williamson et al. (2011), and Reichardt et al. (2012) where the details of the survey strategy, data reduction, and cosmological analysis are also presented. The SPT has now completed a survey of  $2500 \text{ deg}^2$  in the southern hemisphere in three millimeter-wavelength bands. The SPT-SZ survey is essentially complete for clusters with a mass of  $M_{500} \gtrsim 5 \times 10^{14} h_{70}^{-1} M_\odot$  at  $z > 0.3$  and  $M_{500} \gtrsim 3 \times 10^{14} h_{70}^{-1} M_\odot$  at  $z > 1$ .

The SPT-SZ survey has discovered several galaxy clusters that have been spectroscopically confirmed at  $z > 1$  (Brodwin et al. 2010; Foley et al. 2011). Other groups are also discovering high-redshift clusters through X-ray (e.g., Rosati et al. 2004, 2009; Mullis et al. 2005; Stanford et al. 2006; Henry et al. 2010) or infrared imaging (e.g., Stanford et al. 2005, 2012; Brodwin et al. 2006, 2011; Eisenhardt et al. 2008; Muzzin et al. 2009; Wilson et al. 2009; Papovich et al. 2010). However, these techniques do not have the benefit of simultaneously providing the nearly redshift-independent mass selection and wide-area coverage of the SZ technique.

The rich and dense environments of galaxy clusters can also be exploited to study galaxy evolution. They provide a simple way of identifying large populations of galaxies that have similar formation histories. As the redshift of the clusters in the sample increases, earlier phases in the process of galaxy evolution process are observed. With these observations, scenarios of galaxy formation can be tested with less temporal

extrapolation. This also perhaps has ramifications for the hierarchical formation scenario, as the ages of the bright elliptical galaxies may be related to the epoch of the final assembly of the cluster as suggested by semi-analytical simulations such as Dubinski (1998) and Boylan-Kolchin et al. (2009). Recent observations of high-redshift dense environments point to a period of prodigious star formation (Papovich et al. 2012; Snyder et al. 2012) at  $z > 1.3$ , after which the bulk of the galaxy stellar mass build up likely arises from dry mergers (without significant star formation). However, studies of lower-redshift elliptical galaxies suggest that stellar age is minimally affected by environment densities, e.g., Thomas et al. (2010). A larger data set at high redshift is probably required to reconcile these.

SPT-CL J0205–5829 was first identified as a cluster in Reichardt et al. (2012, R12), which describes a catalog of 224 cluster candidates discovered in the first  $720 \text{ deg}^2$  of the  $2500 \text{ deg}^2$  SPT-SZ survey. SPT-CL J0205–5829 was detected with a signal-to-noise ratio of 10.5 in the SPT data. Initial deep optical follow-up observations showed no obvious overdensity of galaxies in  $griz$  images, but additional infrared and *Spitzer* photometry confirmed the presence of extremely red clustered galaxies consistent with a redshift  $z > 1.3$ . Optical spectroscopy of member galaxies confirmed that the cluster is at  $z = 1.322$ . X-ray observations with *XMM-Newton* revealed a luminous and extended X-ray source. Although SPT-CL J0205–5829 is not the most massive SPT cluster, it is the highest-redshift SPT cluster that has been confirmed by spectroscopy to date, and potentially the most massive galaxy cluster known at redshift  $z > 1.2$  (previous to this was XMM2235 from Rosati et al. (2009) at  $z = 1.39$ ), and second most massive at  $z > 1$  (the most massive being SPT-CL J2106–5844 from Foley et al. (2011) at  $z = 1.13$ ).

We present our initial detection and follow-up observations of SPT-CL J0205–5829 in Section 2. In Section 3, we show that SPT-CL J0205–5829 is a massive high-redshift galaxy cluster with a population of normal passively evolving galaxies. We then briefly discuss the implications of the existence of such a massive, evolved cluster at  $z > 1.3$  in Section 4. We summarize and conclude in Section 5. Except where otherwise stated, we assume a flat  $\Lambda\text{CDM}$  cosmology with  $\Omega_M = 0.3$  and  $h_0 = 0.7$  throughout this paper.  $M_{500}$  masses are defined as the mass enclosed in a spherical region which has a density 500 times the critical density of the universe. At  $z = 1.322$ , 1 Mpc subtends 2.0 arcmin and the age of the universe is 4.66 Gyr.

## 2. OBSERVATIONS, DATA REDUCTION, AND INITIAL FINDINGS

### 2.1. Millimeter Observations by the South Pole Telescope

SPT-CL J0205–5829 was initially discovered in the SPT-SZ survey and reported in R12, as part of the cluster catalog identified from the  $720 \text{ deg}^2$  surveyed during the 2008–2009 SPT observing seasons. The survey strategy and data analysis are detailed in the previous SPT-SZ survey papers Staniszewski et al. (2009), Vanderlinde et al. (2010), Williamson et al. (2011, W11), and R12. The SPT-SZ survey was completed in 2011 November, and covers an area of  $2500 \text{ deg}^2$  in three frequency bands at 95, 150, and 220 GHz.

As described in R12, cluster candidates were identified using a multi-band matched-filter approach, similar to that first described by Melin et al. (2006). The significance of a cluster detection (maximized across spatial filter scales and position in map),  $\xi$ , is used to identify cluster candidates. For the survey

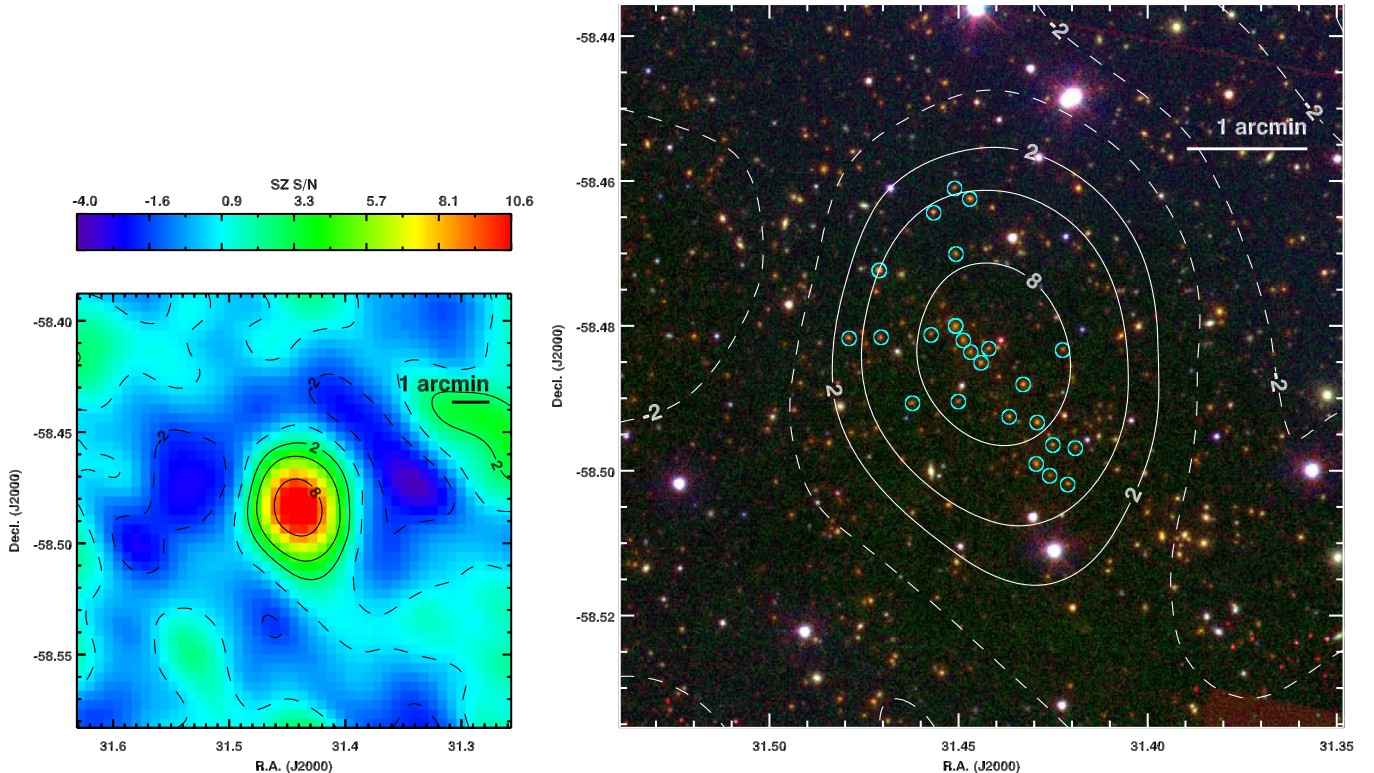


**Figure 1.** Left: the filtered SPT-SZ significance map of SPT-CL J0205–5829. The negative trough surrounding the cluster is an artifact of the filtering of the time-ordered data and maps. Right: color image from IMACS i, NEWFIRM K<sub>s</sub>, *Spitzer*/IRAC [3.6], with SPT-SZ contours overlaid in white and [3.6]–[4.5] color-selected galaxies indicated in cyan.

field containing SPT-CL J0205–5829, only the 95 and 150 GHz data were used, the SPT maps have noise levels of 45 and 16  $\mu$ K arcmin in CMB temperature units at 95 and 150 GHz, respectively. In this data, SPT-CL J0205–5829 was detected with  $\xi = 10.5$  and is among the 5% most significant detections in the R12 catalog. An image of the filtered SPT map is shown in Figure 1.

## 2.2. Optical and Infrared Imaging

We obtained *griz* imaging using the MOSAIC2 imager on the CTIO 4 m Blanco telescope on UT 2010 July 18, 25 and UT 2011 July 4 with mediocre to bad seeing (1''.1–2''.2) and occasional light clouds. Total integration times were 300, 300, 2350, and 1050 s to 10 $\sigma$  point-source depths of 23.8, 23.2, 22.2, and 21.1 AB magnitudes in *g*, *r*, *i*, and *z*, respectively. We also acquired 1800 s of deep *i*-band imaging of SPT-CL J0205–5829 on UT 2011 January 31 with the Inamori Magellan Areal Camera and Spectrograph (IMACS; Dressler et al. 2006) on the Baade Magellan 6.5 m telescope to 24.0 AB magnitude depth in mediocre seeing (1''.2–1''.5). The observation strategy and reduction procedure are described in High et al. (2010, H10), W11, and Song et al. (2012, S12) using the PHOTPIPE pipeline (Rest et al. 2005).

SPT-CL J0205–5829 was also observed with the NEWFIRM imager (Astry et al. 2003) at the CTIO 4 m Blanco telescope on UT 2010 November 6. Data were obtained in the *K<sub>s</sub>* filter under photometric conditions with a 10 $\sigma$  point-source depth of 19.1 Vega magnitudes. At each dither position, 6 frames with 10 s exposure times were co-added at 18 random positions providing a total exposure time of 1080 s. NEWFIRM data were reduced using the FATBOY pipeline, originally developed for the FLAMINGOS-2 instrument, and modified to work with

NEWFIRM data in support of the Infrared Bootes Imaging Survey (A. Gonzalez 2011, private communication). Individual processed frames are combined using SCAMP and SWARP (Bertin et al. 2002), and photometry is calibrated to Two Micron All Sky Survey (Skrutskie et al. 2006). The final image has an FWHM of 0''.96.

Infrared *Spitzer*/IRAC imaging was obtained in 2011 during Cycle 7 as part of a larger program to follow up clusters identified in the SPT survey. IRAC imaging is particularly important for the confirmation and study of high-redshift SPT clusters such as SPT-CL J0205–5829 where the optically faint members are strongly detected in the infrared. The on-target observations consisted of 8  $\times$  100 s and 6  $\times$  30 s dithered exposures in bands [3.6] and [4.5] to 10 $\sigma$  depths of 20.3 and 18.8 Vega magnitudes, respectively. The deep [3.6] observations are sensitive to passively evolving cluster galaxies down to 0.1  $L^*$  at  $z = 1.5$ . The data were reduced exactly as in Brodwin et al. (2010), following the method of Ashby et al. (2009). Briefly, we correct for column pulldown and residual image effects, mosaic the individual exposures, resample to 0''.86 pixels (half the solid angle of the native IRAC pixels), and reject cosmic rays.

## 2.3. Optical Spectroscopy

Multislit spectroscopic observations were acquired for SPT-CL J0205–5829 on the 6.5 m Baade Magellan telescope on UT 2011 September 25–26 using the *f/2* camera on the IMACS spectrograph for a total integration time of 11 hr. The strategy and procedure were as described in Brodwin et al. (2010), with the same 300 l mm<sup>-1</sup> “red” grism and WB6300–9500 filter, but without the GISMO module (in order to increase throughput). The galaxy target selection was based on the optical and infrared photometry; see Section 3. Twenty-two 30 minute exposures were made in excellent to moderately good seeing (0''.4–0''.7)

**Table 1**  
Spectroscopic Members of SPT-CL J0205–5829

ID	R.A. (J2000)	Decl. (J2000)	$z$	$\delta z^a$	Principal Spectral Feature	[O II] Flux <sup>b</sup> ( $\times 10^{-18}$ erg cm $^{-2}$ s $^{-1}$ Å $^{-1}$ )	SFR <sup>b</sup> ( $M_{\odot}$ yr $^{-1}$ )
J020556.50–582730.7	02:05:56.50	−58:27:30.7	1.3219	0.0007	Ca H&K	$2.5 \pm 1.5$	$0.42 \pm 0.28$
J020548.26–582848.4 <sup>c</sup>	02:05:48.27	−58:28:48.4	1.3218	0.0005	Ca H&K	$1.4 \pm 0.9$	$0.24 \pm 0.16$
J020547.70–582855.5	02:05:47.70	−58:28:55.6	1.3239	0.0003	Ca H&K	$1.2 \pm 0.5$	$0.19 \pm 0.11$
J020547.22–582901.5	02:05:47.23	−58:29:01.6	1.3223	0.0005	Ca H&K	$<6.7$	$<1.40$
J020546.57–582907.1	02:05:46.57	−58:29:07.1	1.3230	0.0005 <sup>d</sup>	Ca H&K	$<4.0$	$<0.80$
J020543.00–582936.4	02:05:43.00	−58:29:36.4	1.3119	0.0005	Ca H&K	$<3.4$	$<0.63$
J020543.07–582956.9	02:05:43.08	−58:29:56.9	1.3186	0.0002	Ca H&K	$<1.6$	$<0.28$
J020541.06–583006.9	02:05:41.07	−58:30:07.0	1.3210	0.0007	Ca H&K	$<5.3$	$<0.90$
J020557.04–582713.9	02:05:57.04	−58:27:13.9	1.3106	0.0007	[O II]	$14.8 \pm 4.6$	$2.5 \pm 1.1$

**Notes.**<sup>a</sup> Redshift errors are twice those given by RVSAO.<sup>b</sup> Based on integrated [O II] flux within 4 Å of the line peak with no source extinction correction. Upper limits are  $3\sigma$ .<sup>c</sup> BCG.<sup>d</sup> The RVSAO error was unphysically small and was adjusted up to a typical value.

using one slit mask. The resolution of the observations, as measured from the sky lines, was 5.2 Å. In a procedure identical to J. Ruel et al. (2013, in preparation), the COSMOS reduction package was used for standard CCD processing, resulting in wavelength-calibrated two-dimensional spectra. The one-dimensional spectra were then extracted from the sum of the reduced data. Spectral features were identified by eye from inspection of the two-dimensional and one-dimensional spectra, and redshifts were then obtained by using RVSAO routines.

#### 2.4. X-Ray Observations

A deep X-ray observation of SPT-CL J0205–5829 was obtained by the *XMM-Newton* observatory (ObsID: 0675010101) on UT 2011 June 19–20 using the European Photon Imaging Camera, which consists of two metal-oxide-silicon (MOS) arrays plus one fully depleted p–n (PN) junction CCD array. The total integration times were 69 ks for the MOS arrays and 65 ks for the PN array. The data reduction and analysis were performed with SAS v11.0 utilizing the *XMM-Newton* Extended Source Analysis Software package<sup>34</sup> (e.g., Snowden et al. 2008). The net clean exposure time is 57 and 39 ks in the MOS/PN arrays, respectively. Based on the De Luca & Molendi (2004) diagnostics, we find a  $\sim 30\%$ –40% background enhancement in the observation due to residual quiescent soft proton contamination. The MOS2 CCD#5 was in an anomalously high state and we have removed it from further analysis.

We have also excised all point sources identified in the source detection step. We have visually inspected the excision regions and made conservative adjustments to their size. In particular, a point source associated with a bright galaxy (bluer than the passively evolving model) was identified in the core region of the cluster ( $\alpha = 02:05:45.4$ ,  $\delta = -58:28:58.3$ ,  $\sim 12''$  west of the X-ray centroid) and was removed with an excision radius of  $\sim 11''$  (see Figure 3).

### 3. RESULTS

#### 3.1. Cluster Member Galaxies

From the procedure described in S12, we measure a redshift based on the *Spitzer* IRAC photometry of  $z = 1.30 \pm 0.12$  (see Figure 2). We fit a model of passively evolved galaxies from

Bruzual & Charlot (2003, BC03) to the data to determine the redshift. The optical data were not deep enough to offer any additional constraint to the redshift except for the brightest of the cluster members (see Section 3.3). The redshift estimator identified 32 galaxies with IRAC [3.6]–[4.5] colors consistent with this redshift (a  $3.5\sigma$  overdensity compared to the background), shown in Figures 1 and 2. From this list, we designed a multi-slit mask for the IMACS spectroscopic observations described in Section 2.3, filling the mask with other targets, identified as galaxies with bluer colors relative to the model in the *i* band and *Spitzer* data.

#### 3.2. Spectroscopy

Redshifts and other spectroscopic properties of member galaxies are listed in Table 1. Of the 47 slits designed into the mask, 1 spectroscopic member was identified from an [O II] emission line, and 8 from Ca H and K. Figure 3 shows the spectra of the 9 cluster members. The brightest cluster galaxy (BCG), defined as the brightest cluster member in [3.6], is at a redshift of  $z = 1.3218 \pm 0.0005$ , and the combined robust (biweight) redshift of nine cluster members is  $z = 1.322^{+0.001}_{-0.002}$ . We do not calculate the velocity dispersion due to the overwhelming intrinsic uncertainty in the derived mass estimates with  $< 15$  members (Saro et al. 2012).

We also estimate the star formation rate (SFR) for each cluster member from the integrated [O II] flux which was corrected for galactic extinction (reddening) using the dust map from Schlegel et al. (1998) and scaled to match the *i*-band magnitude from IMACS imaging. We do not correct for source dust extinction as we lack a well-constrained NUV-Blue-continuum measurement for most of these galaxies. This is also consistent with our derived extinction from spectral energy distribution (SED) fits of the four brightest central galaxies (see Section 3.3). We measured the continuum-subtracted flux centered on the [O II] wavelength with a bin width of 8 Å (320 km s $^{-1}$ ) and converted to luminosity using the cluster redshift. The SFR was estimated from the [O II] luminosity using the scaling law from Kennicutt (1998). The measured [O II] flux and SFR (or  $3\sigma$  upper limits) are given in Table 1.

#### 3.3. Brightest Central Galaxies

We selected the brightest central galaxies to be the four brightest galaxies consistent with the [3.6]–[4.5] model, within

<sup>34</sup> [http://heasarc.gsfc.nasa.gov/docs/xmm/xmmhp\\_xmmesas.html](http://heasarc.gsfc.nasa.gov/docs/xmm/xmmhp_xmmesas.html)

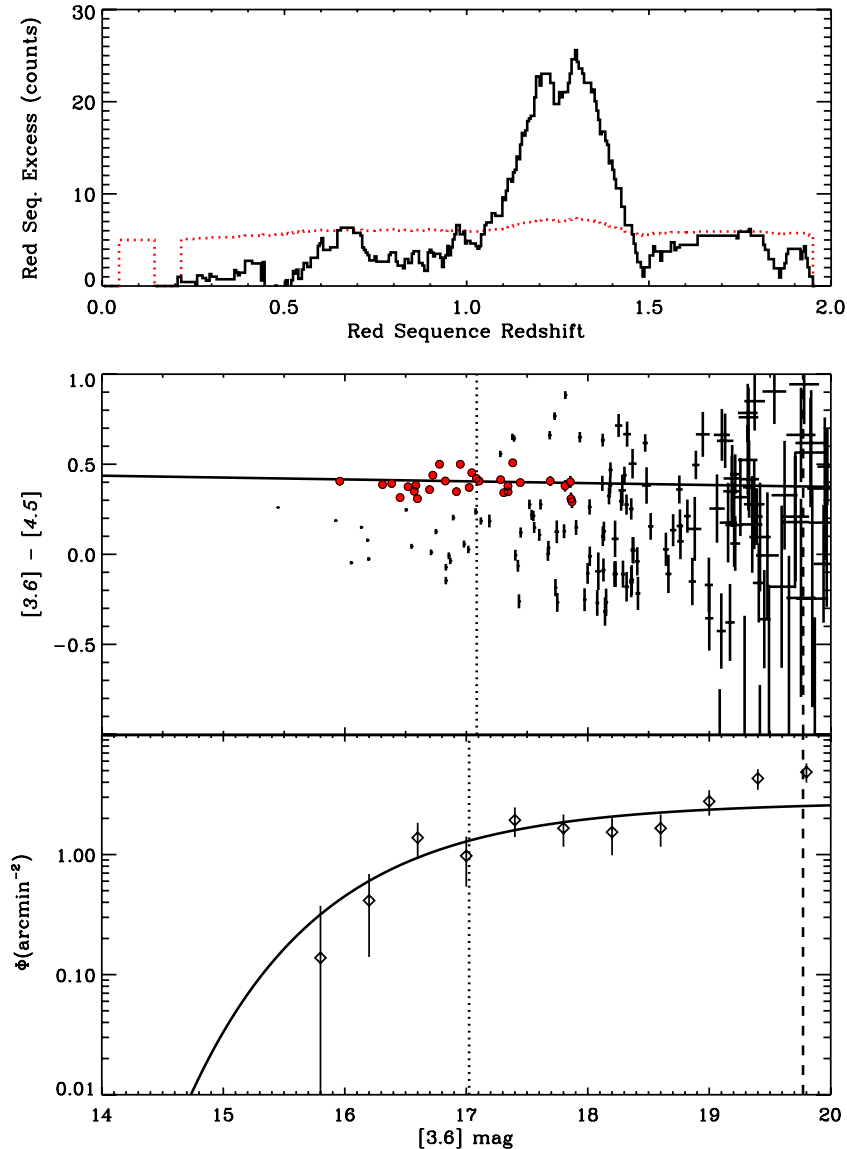


**Figure 2.** Cluster member finding for SPT-CL J0205–5829. The top panel shows the excess of surface density of galaxies (above background) consistent within  $2\sigma$  of the SED model as a function of redshift. The rms level of the overdensity is shown in dotted red. The peak overdensity is at  $z = 1.30$  at  $3.5\sigma$  above the background rms. The middle panel shows the color–magnitude diagram of all objects within 2 arcmin of the SPT center coordinates with red-filled black circles showing the selected galaxies from the passively evolving model at  $z = 1.30$  (black solid line) and brighter than  $m^*+1$ . The inferred model  $m^*$  is shown as a dotted vertical line and the [3.6] mag limit is shown as the dashed line. The bottom panel shows the *Spitzer* [3.6] galaxy luminosity function for SPT-CL J0205–5829. The dotted vertical line shows the best-fit  $m^*$  in [3.6], and the dashed line shows the [3.6] mag limit.

(A color version of this figure is available in the online journal.)

1 arcmin of the SZ center. We then use an analysis similar to the Rosati et al. (2009) SED fitting procedure. To constrain the SFH of each of these galaxies, we fit an exponential-burst stellar population SED model at solar metallicity and Chabrier initial mass function from BC03 to the available photometry (see Figure 4), including magnitude lower limits, fix the redshift at  $z = 1.322$ , and add a source reddening model from Calzetti et al. (2000). From the fit parameters, we calculate the rest-frame  $K$ -band luminosity, stellar mass (and corresponding stellar mass-to-light ratios), and age. The uncertainties for these parameters are from the  $\chi^2$  68% confidence intervals in the multi-dimensional sampled grid and checked by bootstrapping this procedure hundreds of times and were in good agreement. These parameters are presented in Table 2. We find that all models give well-constrained  $K$ -band luminosities, mainly because the observed *Spitzer* [4.5] filter corresponds to  $2 \mu\text{m}$  in

the rest frame. The  $4000 \text{\AA}$  breaks are mainly constrained by the deep IMACS  $i$ -band measurement.

The rest-frame  $K$ -band luminosity of the brightest galaxy, at  $L \sim 4 \times 10^{11} L_\odot$ , is typical for BCGs in similar-sized clusters at  $z < 0.25$  based on previous X-ray (Haarsma et al. 2010) or optical cluster studies (Lin & Mohr 2004; Popesso et al. 2007; Brough et al. 2008), and smaller studies extending to higher redshifts ( $z < 1$ ) by Whiley et al. (2008). The derived stellar mass is also consistent with other studies of BCGs from X-ray samples at similar cluster masses and redshifts (Stott et al. 2010). The derived ages from the BC03 model fits listed in Table 2 suggest that the stellar mass of these brightest galaxies had formed by the time of the observed epoch was probably complete by redshift 2 or 3, or perhaps earlier, also consistent with previous studies of stellar ages of cluster galaxies at high redshift (Collins et al. 2009; Henry et al. 2010). However, this

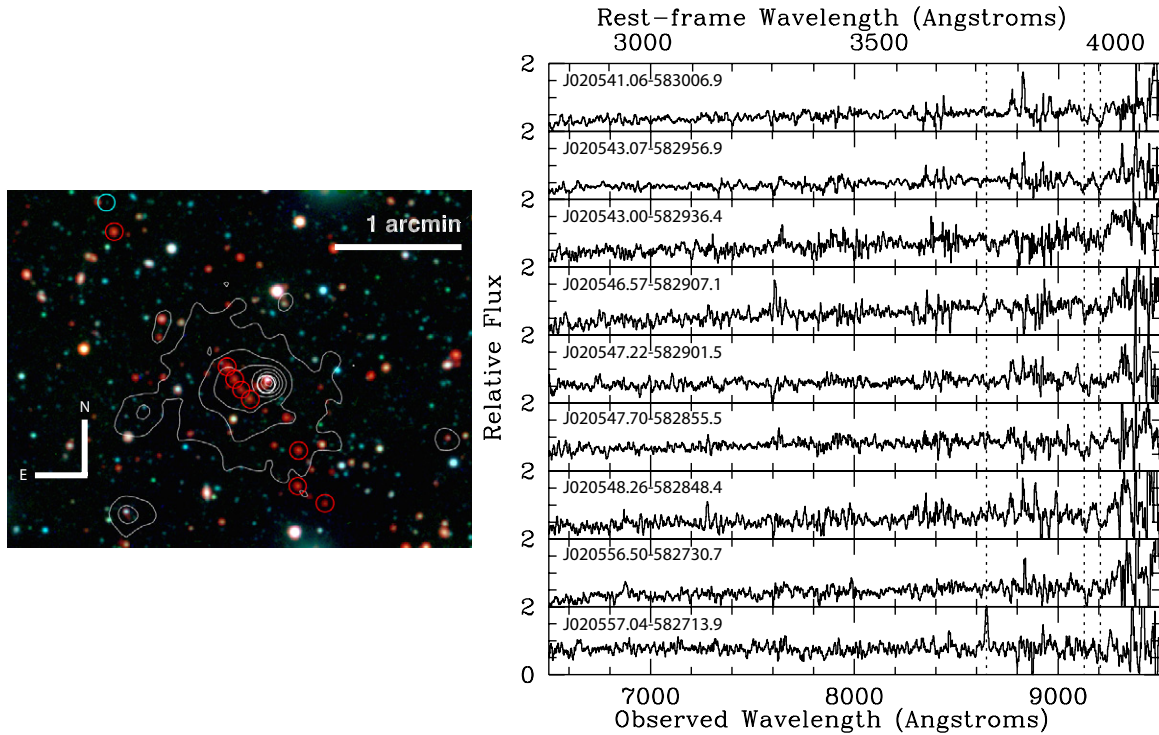


**Figure 3.** Left: optical ( $r/i$ ) and *Spitzer*/IRAC [3.6] image showing the galaxies confirmed by spectroscopy and overlaid by the *XMM-Newton* X-ray contours. Cyan shows the [O II] detection shown to the right (bottom panel), and red shows the members identified with Ca H and K features shown to the right. The white circle shows the X-ray point-source position. The frame subtends  $4.5 \times 3.4$  arcmin. Right: spectra of all nine member galaxies with the [O II] and Ca H and K features indicated in vertical dotted lines. Despite the long exposure time on Magellan, these features are faint due to the red color of passively galaxies.

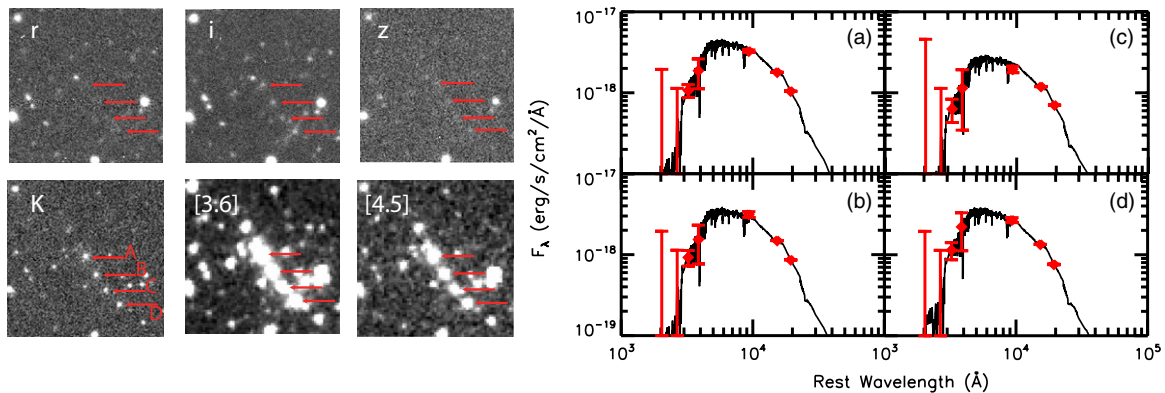


**Figure 4.** Best BC03 models for the four brightest galaxies in the central region of SPT-CL J0205–5829. The left panel shows thumbnails of six observed filters ( $r, i, z, K_s, [3.6]$ , and  $[4.5]$ ) in the central  $\sim 30''$  from the brightest galaxy (A), with the four galaxies labeled in the  $K_s$  image. The right panels show the measured photometry in red with the best-fit BC03 model for each overplotted.

does not rule out the scenario of “dry merging” hierarchical build up of these galaxies between redshift 1.3 and 3.

### 3.4. NIR Luminosity Function

As a further check on the cluster galaxy properties, we measure the observed [3.6] (roughly rest  $H$  band) luminosity function of galaxies with [3.6]–[4.5] colors consistent with the BC03 model from our initial redshift estimate. Galaxies selected as cluster members are within 1 Mpc (physical distance) of the SZ-derived center and have [3.6]–[4.5] colors within  $2\sigma$  (based on each galaxy’s photometric uncertainty) of the BC03 model. We then measure the number density in 0.4 mag bins from the BCG to 1 mag brighter than the measured  $10\sigma$  magnitude limit (to reduce any systematic errors due to incompleteness

in the catalog). Field galaxy contamination was corrected by measuring the same quantity outside of the 1 Mpc aperture and subtracting. We used the Schechter luminosity function

$$\Phi(m) = 0.4 \ln(10) \Phi^* 10^{-0.4\mu(\alpha+1)} \exp(-10^{-0.4\mu}), \quad (1)$$

where  $\mu = m - m^*$  and allowed  $\Phi^*$ ,  $\alpha$ , and  $m^*$  to vary. The final derived parameters and uncertainties are from the least-squares fit to the data and bootstrapping the whole procedure thousands of times from the catalog selection stage. We found the [3.6] best-fit parameters are  $\Phi^* = 2.73 \pm 0.31$  arcsec<sup>-2</sup>,  $\alpha = -1.02 \pm 0.11$  and  $m^* = 16.58 \pm 0.29$  (Vega), which are roughly consistent with our previous model assumptions of  $\alpha = -1.0$  and  $m^* = 17.09$  at this redshift, calculated from the evolving stellar population BC03 models, normalized to the

**Table 2**  
Brightest Central Galaxy Parameters

Galaxy	$M_{\text{stellar}}^{\text{a}}$ ( $10^{11} M_{\odot}$ )	$M_K^{\text{b}}$ (Vega)	$L_K^{\text{c}}$ ( $10^{11} L_{\odot}$ )	$M/L^{\text{d}}$ ( $M_{\odot}/L_{\odot}$ )	Age <sup>e</sup> (Gyr)	$\tau^{\text{f}}$ (Gyr)	$A_V^{\text{g}}$
A	$3.5 \pm 0.5$	$-25.51 \pm 0.05$	$3.3 \pm 0.2$	$1.1 \pm 0.2$	$4.5 \pm 0.5$	$0.1 \pm 0.1$	$0.0 \pm 0.1$
B	$2.9 \pm 0.5$	$-25.31 \pm 0.05$	$2.7 \pm 0.2$	$1.1 \pm 0.2$	$4.5 \pm 0.8$	$0.1 \pm 0.1$	$0.0 \pm 0.1$
C	$2.3 \pm 0.4$	$-25.07 \pm 0.12$	$2.2 \pm 0.3$	$1.1 \pm 0.4$	$4.5 \pm 0.6$	$0.1 \pm 0.2$	$0.1 \pm 0.2$
D	$1.9 \pm 0.3$	$-25.19 \pm 0.08$	$2.4 \pm 0.2$	$0.8 \pm 0.2$	$2.8 \pm 0.9$	$0.1 \pm 0.2$	$0.0 \pm 0.1$

**Notes.**<sup>a</sup> Model initial stellar mass at  $t = t_{\text{form}}$ .<sup>b</sup> Absolute rest-frame  $K$  magnitude at  $t = t_{\text{obs}}$ .<sup>c</sup> Rest-frame  $K$  luminosity at  $t = t_{\text{obs}}$ .<sup>d</sup> Stellar mass to  $K$  luminosity ratio.<sup>e</sup>  $t_{\text{obs}} - t_{\text{form}}$ .<sup>f</sup>  $e$ -folding timescale for  $\text{SFR} \propto \exp(t/\tau)$ .<sup>g</sup> Rest-frame  $V$ -band extinction in magnitudes.

**Table 3**  
Mass Estimates for SPT-CL J0205–5829

Observable	Measurement	$M_{500}$ ( $10^{14} h_{70}^{-1} M_{\odot}$ )
SZ $\xi$	10.5	<b>4.8 ± 1.0</b>
SZ $\xi$ (flat prior)	10.5	$5.2 \pm 1.1$
$T_X$	$8.7^{+1.0}_{-0.8}$ keV	$5.2 \pm 1.3$
<b>Combined</b>	...	<b>4.8 ± 0.8</b>

**Notes.** Unbolded masses indicate Eddington-biased mass estimates, calculated using flat priors on mass. Note that the SZ (untargeted) flat-prior measurement suffers from a considerably different Eddington bias than the  $T_X$  (targeted) flat-prior estimate. The  $T_X$  mass estimate and the unbiased SZ  $\xi$  mass estimate were used to generate the combined mass estimate based on their probability distributions (see Section 3.7).

Coma cluster luminosity function (see H10 for a discussion). Recent measurements of the luminosity function in evolved  $z > 1$  clusters find a similarly flat faint-end slope,  $\alpha$  (Mancone et al. 2012). In contrast, less-evolved high-redshift clusters have a paucity of faint galaxies, indicated by a shallower faint-end slope (e.g., Rudnick et al. 2012; Lemaux et al. 2012).

This best-fit luminosity function also corresponds to a richness measurement of  $N_{\text{gal}} = 47 \pm 4$  using the H10 procedure (integrating the luminosity function down to  $m^* + 1$  within a 1 Mpc physical radius of the BCG) and is consistent with the H10 sample of SPT-SZ clusters which are drawn from the same SPT-SZ significance although sampled at a different wavelength (observed  $i$  band).

### 3.5. SZ Mass Estimate

We use an SZ mass estimate as described in R12 and Benson et al. (2011), which is calculated from the Markov chain Monte Carlo method using available CMB, BAO, SNe, and SPT-CL (from the R12 cluster sample) data. The masses reported are posterior estimates based on the probability density function using the  $\xi$  and redshift for SPT-CL J0205–5829, marginalized over uncertainties in the SZ and X-ray ( $Y_X$ ) observable-mass scaling relations and cosmology. In Table 3, we quote mass estimates with and without a Bayesian prior assumption on the underlying population of clusters. The expected bias on the flat-prior mass estimate is related to Eddington bias and affects the SPT-CL J0205–5829 mass estimate at the  $\sim 10\%$  level. This bias is due to the steeply falling mass function which makes it more likely for SPT-CL J0205–5829 to be a lower mass

cluster that scattered up than a higher mass cluster scattering down. The total uncertainty in mass ( $\sim 20\%$ ) is dominated a combination of the intrinsic scatter and the uncertainty in the normalization of the SZ–mass scaling relation. In Table 3, the mass estimates are given as  $M_{500}$ , defined as the mass within a radius in which the cluster has a density 500 times the critical density of the universe. We can convert between this  $M_{500}$  and  $M_{200}$  with respect to  $\rho_{\text{mean}}$ , defined as the mass within a radius in which the cluster has a density 200 times the mean density of the universe, by assuming a Navarro–Frenk–White profile (Navarro et al. 1997) and the mass–concentration relation by Duffy et al. (2008). Using this conversion, the  $M_{200}$  masses are a factor of  $\sim 1.8$  times larger, such that the unbiased SZ mass estimate is  $M_{200} = (8.7 \pm 1.8) \times 10^{14} h_{70}^{-1} M_{\odot}$ .

### 3.6. X-Ray Spectroscopy with XMM-Newton

We estimate the X-ray physical parameters of SPT-CL J0205–5829 using an iterative process over the cluster radius. We measure the core-excised X-ray temperature,  $T_X$ , within  $r_{500}$ , defined as the radius inside which the mass density is higher than 500 times the critical density of the universe. We iterate over values of  $r_{500}$  so that the measured  $T_X$  maintains consistency with the  $M - T$  relation from Vikhlinin et al. (2009, V09).

For each value of  $r_{500}$ , we extract spectra and redistribution and ancillary response files. We excise all detected point sources from both the source and background regions as well as the central  $r \leq 0.15 r_{500}$  cluster core region. Given the significant residual quiescent contamination (Section 2.4), we opt to use a local background model in the fitting procedure. For each camera, we subtract a background spectrum extracted from an annulus centered on the cluster between  $160''$  and  $320''$  in radius. These radii were selected based on the cumulative count rate profiles so that the annulus is not contaminated by cluster emission while still lying on the same MOS chips as the source. The total number of background-subtracted source counts is  $\sim 5500$  for all three cameras. We use Xspec v12.5 to fit the spectra with a MeKaL model (Mewe et al. 1985; Kaastra et al. 1992; Liedahl et al. 1995) using  $C$ -statistics on minimally binned spectra (i.e., binning only channels to obtain  $\geq 1$  counts  $\text{bin}^{-1}$ ). From this fit to the spectrum, we measure the X-ray temperature.

We then use the measured X-ray temperature and the redshift from optical spectroscopy to infer an  $M_{500}$  mass from the V09  $M - T$  relation, which we also convert to a corresponding  $r_{500}$  value. Given this new value of  $r_{500}$ , we iterate on this process

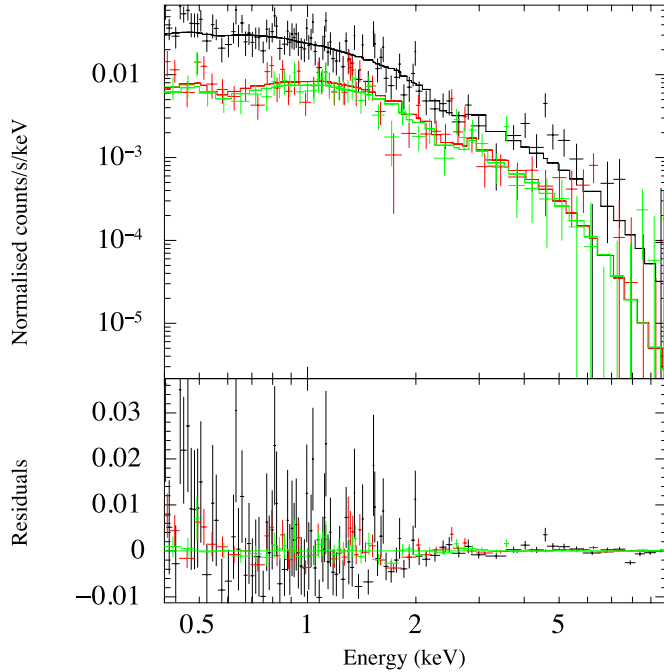


**Figure 5.** X-ray spectrum of SPT-CL J0205–5829 (black: PN; green: MOS1; red: MOS2).

until two successive  $r_{500}$  estimates differ by  $\leq 2''.5$  (equal to the bin size of our X-ray images). This criterion was reached in four iterations and we have verified that the final solution is independent of the initial  $r_{500}$  value. The  $r_{500}$  radius is 710 kpc ( $\sim 85''$ ) and the excised core region (i.e.,  $0.15 r_{500}$ ) has a radius of  $\sim 13''$  (roughly twice the point spread function (PSF) FWHM).

The final spectrum is displayed in Figure 5. The best-fit temperature is  $T_X = 8.7^{+1.0}_{-0.8}$  keV. This corresponds to a mass of  $M_{500} = (5.2 \pm 1.3) \times 10^{14} h_{70}^{-1} M_\odot$  using the relation from V09. There is no evidence that SPT-CL J0205–5829 is unrelaxed from the X-ray morphology or the galaxy distributions, either on the sky or in the velocities, therefore we use the standard  $M - T$  relation from V09 and make no corrections based on the dynamical state of the cluster. In the  $T_X$ -based mass estimate, we include the statistical uncertainty in the measurement of  $T_X$ , uncertainties in cosmology, and assume a 20% intrinsic scatter in the  $M - T$  relation, as noted by V09.

We constrain the mean [Fe] abundance to  $Z = 0.26 \pm 0.15 Z_\odot$  which is consistent with a typical mean metallicity for the ICM in a massive galaxy cluster ( $Z \sim 0.3 Z_\odot$ ) at lower redshifts (e.g., Matsumoto et al. 2000; Tozzi et al. 2003; Maughan et al. 2008). The luminosity within  $r_{500}$  is  $L_X(0.5\text{--}2.0 \text{ keV}) = (3.91 \pm 0.05) \times 10^{44} \text{ erg s}^{-1}$  in the rest frame.

We also note that we detect the Fe K line clearly in PN and MOS2 and more weakly in MOS1. If we allow the redshift to vary during fitting the best-fit value from the joint fit is  $z = 1.39 \pm 0.02$ , which is  $\sim 5\%$  larger than the optical spectroscopic redshift of  $z = 1.322^{+0.001}_{-0.002}$ . The redshifts derived from individual cameras are  $1\sigma$  consistent with the joint PN+MOS1+MOS2 fit (except MOS1 which gives a slightly lower redshift). This is one of the highest redshifts measured from X-ray spectra (cf. Lloyd-Davies et al. 2011).

### 3.7. Combined Mass Estimate

We follow Foley et al. (2011) and calculate a joint estimate using the SZ mass and X-ray mass estimates of SPT-CL

J0205–5829. We assume the uncertainties are uncorrelated between the two masses. This allows for a more straightforward evaluation of the posterior probability distribution function (PDF),

$$P(M|\xi, T_X) \propto P(M)P(\xi|M)P(T_X|M), \quad (2)$$

where  $P(M)$  is the Tinker halo mass function (Tinker et al. 2008),  $P(\xi|M)$  is the flat-prior SZ mass estimate PDF, and  $P(T_X|M)$  is the flat-prior  $T_X$  mass estimate PDF. As calculated in Sections 3.5 and 3.6, we use the X-ray and SZ mass estimates derived from the observables  $T_X$  and  $\xi$ , respectively, which were marginalized over uncertainties in their scaling relations and cosmology. We find a combined, unbiased, mass estimate to be  $M_{500} = (4.8 \pm 0.8) \times 10^{14} h_{70}^{-1} M_\odot$ . Converting to  $M_{200}$  as above gives  $M_{200} = (8.8 \pm 1.4) \times 10^{14} h_{70}^{-1} M_\odot$ .

## 4. DISCUSSION

The galaxy members in SPT-CL J0205–5829 were identified via [3.6]–[4.5] color, and the significant overdensity of these is how this cluster was initially confirmed after it was identified by the SZ effect. The measured overdensity (richness) of these galaxies is consistent with other SPT-SZ clusters, a sample that has a median mass of  $M_{500} \sim 3.3 \times 10^{14} h_{70}^{-1} M_\odot$ . From SED fitting, the BCG and three other bright central galaxies have luminosities and stellar masses typical of central galaxies in clusters of similar mass at lower redshift and have derived stellar population ages greater than  $\sim 3$  Gyr. This suggests that most of the eventual stellar mass in these galaxies are already present at  $z = 1.3$  and the vast majority of these stars were formed by  $z \sim 3$ . The actual assembly scenario of these galaxies cannot be constrained yet.

The quiescent SEDs and the amount of [O II] in the spectra of the central galaxies suggest there is very little ongoing star formation ( $< 0.5 M_\odot \text{ yr}^{-1}$ ) in the center of SPT-CL J0205–5829, meaning there is no *strong* cooling flow mechanism depositing new gas into these galaxies (Hu et al. 1985; Heckman et al. 1989; Crawford et al. 1999; Hatch et al. 2007; McDonald et al. 2010). However, it should be noted that only a very strong cooling core would be discernible in [O II] (McDonald 2011; Santos et al. 2011) and a better indicator would be  $H_\alpha$ . The central X-ray point source noted in Section 2.4 could possibly be a central active galactic nucleus (AGN) that is suppressing the star formation in the cluster. Alternatively, given the age of the cluster and the X-ray cooling time, there might not have been sufficient time for a strong cooling flow to form. Either interpretation is consistent with the general lack of star formation and strong cooling flows at  $z > 0.5$  found in previous studies (Santos et al. 2008; Vikhlinin et al. 2007; Samuele et al. 2011; McDonald 2011), where the number density of strong cooling flows increases dramatically at  $z < 0.5$  while AGN and merger activity decreases. We do not see any indication of a major merger either in the X-ray morphology or galaxy distribution.

From the X-ray spectrum, we found that the cluster gas has a metallicity consistent, albeit with significant uncertainty, with massive clusters at lower redshift. This is also consistent with several studies (see Baldi et al. 2012 for a review) of ICM metal abundances over a range of redshifts that found little or no evidence of evolution from  $z < 1.4$ . Several studies have found that this enrichment can happen over a timescale of 1 Gyr (Pipino & Matteucci 2004) and settle into the central region within a cluster crossing time (1 Gyr). The best-fit metallicity of SPT-CL J0205–5829 would suggest that the bulk of the metal production

could have been completed by  $z \sim 2.5$ ; however, more X-ray observations are needed to say this with high statistical significance.

The optical and infrared data have shown that the stellar populations of the most massive central galaxies are already well evolved, suggesting that the assembly of these galaxies happened within the preceding 2–4 Gyr. It has been suggested that this timeline may depend on the mass of the cluster, as there is some evidence that the BCGs at  $z > 1$  in lower mass clusters have not fully assembled (Stott et al. 2010). It may become possible to see this change over the full SPT mass range and may probe different regimes where other feedback modes dominate. Such a study of a large SZ-selected sample has the potential to directly measure the build up of the stellar mass as a function of redshift and cluster mass.

#### 4.1. Rarity

Although SPT-CL J0205–5829 was included in the sample used in R12 for cosmological analysis, we did not assign a goodness of fit to the model, so it is interesting to quantify the probability of having found this cluster in the full 2500 deg $^2$  SPT-SZ survey. We use the full 2500 deg $^2$  SPT-SZ survey area in order to avoid a posteriori selection of the area in which SPT-CL J0205–5829 was found, which could artificially boost the apparent rarity. We follow Foley et al. (2011) and compute the probability of finding a cluster at higher mass and higher redshift than SPT-CL J0205–5829. We do so by sampling the cosmological and scaling relation constraints of the CMB+BBN+BAO+HST+SN+SPT<sub>CL</sub> chain from R12 and producing a posterior statistical mass estimate  $P(M|\xi, z)$  at each step in the chain. We then compute the expected number of clusters at higher mass and higher redshift

$$\tilde{x}_{>z>M} = \int_0^\infty \int_z^\infty \frac{dN}{dM'dz'} \int_0^{M'} P(M''|\xi, z) dM'' dz' dM', \quad (3)$$

where  $dN/dMdz$  is the mass function as calculated following Tinker et al. (2008). The median point in cosmological and scaling relation parameter space predicts  $\tilde{x}_{>z>M} = 0.07$  clusters at higher mass and higher redshift than SPT-CL J0205–5829 in 2500 deg $^2$ .

However, as noted by Hotchkiss (2011), Hoyle et al. (2012), and Waizmann et al. (2012a, 2012b), this statistic has a small expectation value due to the fact that it requires a cluster of simultaneously higher mass and higher redshift than a particular object. This statistic does not consider the fact that many similarly rare clusters could exist with a slightly higher mass and lower redshift or lower mass and higher redshift. Instead, we follow the treatment of Hotchkiss (2011) and compute the probability of finding the particular value of  $\tilde{x}_{>z>M} = 0.07$ , corresponding to SPT-CL J0205–5829 for an ensemble of simulated 2500 deg $^2$  surveys. We then create a normalized histogram of the resulting values of  $\tilde{x}_{>z>M}$  for the rarest cluster in each catalog and integrate the area under the curve from 0 to the value of  $\tilde{x}_{>z>M}$  for the particular cluster in question. This statistic, unlike  $\tilde{x}_{>z>M}$  itself, has an expectation value of 0.5. We note that it depends only very weakly on the details of the simulation or the point in cosmological or scaling relation space at which the simulations are performed. This metric suggests that this cluster is not at all surprising with a probability of 0.69 of finding at least one cluster as rare as SPT-CL J0205–5829 in 2500 deg $^2$ .

As a comparison to other more rare clusters in the SPT-SZ survey, using the same statistic we find 0.21 for SPT-CL J2106–5844, which was considered in Foley et al. (2011) and 0.05 for SPT-CL J0102–4915 (ACT-CL 0102-4915), currently the rarest cluster in 2500 deg $^2$  SPT-SZ survey.

## 5. SUMMARY AND CONCLUSIONS

We report the massive galaxy cluster SPT-CL J0205–5829 at  $z = 1.322$  discovered in the first 720 deg $^2$  of the SPT-SZ survey and present results of follow-up observations at optical, infrared, and X-ray wavelengths. The galaxy population of this cluster shows a strong red sequence with a luminosity function consistent with that of lower-redshift SZ-selected clusters. Galaxy SED fits to an exponentially decaying SFR stellar population, the [Fe] abundance from the X-ray spectrum, and the lack of [O II] emission in most of the optical galaxy spectra suggest that the bulk of the star formation happened at an earlier epoch ( $z > 2.5$ ). Optical spectroscopy of nine galaxies confirms the cluster redshift at  $z = 1.322^{+0.001}_{-0.002}$ , also roughly consistent with X-ray spectroscopy which gives  $z = 1.39 \pm 0.02$ . This establishes SPT-CL J0205–5829 as the highest-redshift SZ-selected galaxy cluster verified by spectroscopy, and the second most massive SZ-selected cluster known at  $z > 1$ . Based on the X-ray temperature, SPT-CL J0205–5829 is consistent with being more massive than XMM2235 at  $z = 1.39$  with  $T_X = 8.6^{+1.3}_{-1.2}$  from Rosati et al. (2009; but the uncertainties in both temperatures are much larger than the measured difference).

The measured mass observables (from the SZ and X-ray temperature) are consistent and give a combined mass estimate of  $M_{500} = (4.8 \pm 0.8) \times 10^{14} h_{70}^{-1} M_\odot$ . Although not the most massive SZ-discovered cluster, it demonstrates that a cluster of this mass has enough time to form during the first 5 Gyr of the universe, and the existence of this rare object appears to be fully consistent with general expectations for a flat  $\Lambda$ CDM cosmological model.

In general, we find that SPT-CL J0205–5829 has properties similar to clusters with the same mass at lower redshift. This is extremely important in the context of an ultimate goal of an unbiased and low scatter mass calibration of clusters over a wide range of redshifts for cosmological studies, and provides new insight to the assembly of the rarest and most massive structures in the universe.

The South Pole Telescope program is supported by the National Science Foundation through grant ANT-0638937. Partial support is also provided by the NSF Physics Frontier Center grant PHY-0114422 to the Kavli Institute of Cosmological Physics at the University of Chicago, the Kavli Foundation, and the Gordon and Betty Moore Foundation. Galaxy cluster research at Harvard is supported by NSF grant AST-1009012. Galaxy cluster research at SAO is supported in part by NSF grants AST-1009649 and MRI-0723073. The McGill group acknowledges funding from the National Sciences and Engineering Research Council of Canada, Canada Research Chairs program, and the Canadian Institute for Advanced Research. X-ray research at the CfA is supported through NASA Contract NAS 8-03060. The Munich group acknowledges support from the Excellence Cluster Universe and the DFG research program TR33. This work is based in part on observations obtained with the *Spitzer Space Telescope* (PID 60099), which is operated by the Jet Propulsion Laboratory, California Institute of Technology under a contract with NASA. Support for this work was

provided by NASA through an award issued by JPL/Caltech. Additional data were obtained with the 6.5 m Magellan Telescopes located at the Las Campanas Observatory, Chile and the Blanco 4 m Telescope at Cerro Tololo Inter-American Observatories in Chile. R.J.F. is supported by a Clay Fellowship. B.A.B is supported by a KICP Fellowship. M. Bautz acknowledges support from contract 2834-MIT-SAO-4018 from the Pennsylvania State University to the Massachusetts Institute of Technology. M.D. acknowledges support from an Alfred P. Sloan Research Fellowship. W.F. and C.J. acknowledge support from the Smithsonian Institution.

## REFERENCES

- Ashby, M. L. N., Stern, D., Brodwin, M., et al. 2009, *ApJ*, **701**, 428  
 Autry, R. G., Probst, R. G., Starr, B. M., et al. 2003, *Proc. SPIE*, **4841**, 525  
 Baldi, A., Ettori, S., Molendi, S., et al. 2012, *A&A*, **537**, A142  
 Benson, B. A., de Haan, T., Dudley, J. P., et al. 2011, arXiv:1112.5435  
 Bertin, E., Mellier, Y., Radovich, M., et al. 2002, in ASP Conf. Ser. 281, Astronomical Data Analysis Software and Systems XI, ed. D. A. Bohlender, D. Durand, & T. H. Handley (San Francisco, CA: ASP), 228  
 Boylan-Kolchin, M., Springel, V., White, S. D. M., Jenkins, A., & Lemson, G. 2009, *MNRAS*, **398**, 1150  
 Brodwin, M., Brown, M. J. I., Ashby, M. L. N., et al. 2006, *ApJ*, **651**, 791  
 Brodwin, M., Ruel, J., Ade, P. A. R., et al. 2010, *ApJ*, **721**, 90  
 Brodwin, M., Stern, D., Vikhlinin, A., et al. 2011, *ApJ*, **732**, 33  
 Brough, S., Couch, W. J., Collins, C. A., et al. 2008, *MNRAS*, **385**, L103  
 Bruzual, G., & Charlot, S. 2003, *MNRAS*, **344**, 1000  
 Calzetti, D., Armus, L., Bohlin, R. C., et al. 2000, *ApJ*, **533**, 682  
 Carlstrom, J. E., Ade, P. A. R., Aird, K. A., et al. 2011, *PASP*, **123**, 568  
 Carlstrom, J. E., Holder, G. P., & Reese, E. D. 2002, *ARA&A*, **40**, 643  
 Colafrancesco, S., Lucchin, F., & Matarrese, S. 1989, *ApJ*, **345**, 3  
 Collins, C. A., Stott, J. P., Hilton, M., et al. 2009, *Natur*, **458**, 603  
 Crawford, C. S., Allen, S. W., Ebeling, H., Edge, A. C., & Fabian, A. C. 1999, *MNRAS*, **306**, 857  
 De Luca, A., & Molendi, S. 2004, arXiv:astro-ph/0402233  
 Dressler, A., Hare, T., Bigelow, B. C., & Osip, D. J. 2006, *Proc. SPIE*, **6269**, 62690F  
 Dubinski, J. 1998, *ApJ*, **502**, 141  
 Duffy, A. R., Schaye, J., Kay, S. T., & Dalla Vecchia, C. 2008, *MNRAS*, **390**, L64  
 Eisenhardt, P. R. M., Brodwin, M., Gonzalez, A. H., et al. 2008, *ApJ*, **684**, 905  
 Foley, R. J., Andersson, K., Bazin, G., et al. 2011, *ApJ*, **731**, 86  
 Haarsma, D. B., Leisman, L., Donahue, M., et al. 2010, *ApJ*, **713**, 1037  
 Hatch, N. A., Crawford, C. S., & Fabian, A. C. 2007, *MNRAS*, **380**, 33  
 Heckman, T. M., Baum, S. A., van Breugel, W. J. M., & McCarthy, P. 1989, *ApJ*, **338**, 48  
 Henry, J. P., Salvato, M., Finoguenov, A., et al. 2010, *ApJ*, **725**, 615  
 High, F. W., Stalder, B., Song, J., et al. 2010, *ApJ*, **723**, 1736  
 Hotchkiss, S. 2011, *JCAP*, **07**, 004  
 Hoyle, B., Jimenez, R., Verde, L., & Hotchkiss, S. 2012, *JCAP*, **02**, 009  
 Hu, E. M., Cowie, L. L., & Wang, Z. 1985, *ApJS*, **59**, 447  
 Kaastra, J. S., Asaoka, I., Koyama, K., & Yamauchi, S. 1992, *A&A*, **264**, 654  
 Kennicutt, R. C., Jr. 1998, *ARA&A*, **36**, 189  
 Lemaux, B. C., Gal, R. R., Lubin, L. M., et al. 2012, *ApJ*, **745**, 106  
 Liedahl, D. A., Osterheld, A. L., & Goldstein, W. H. 1995, *ApJL*, **438**, 115  
 Lin, Y.-T., & Mohr, J. J. 2004, *ApJ*, **617**, 879  
 Lloyd-Davies, E. J., Romer, A. K., Mehrtens, N., et al. 2011, *MNRAS*, **418**, 14  
 Lucchin, F., & Matarrese, S. 1988, *ApJ*, **330**, 535  
 Mancone, C. L., Baker, T., Gonzalez, A. H., et al. 2012, *ApJ*, **761**, 141  
 Marriage, T. A., Acquaviva, V., Ade, P. A. R., et al. 2011, *ApJ*, **737**, 61  
 Matsumoto, H., Tsuru, T. G., Fukazawa, Y., Hattori, M., & Davis, D. S. 2000, *PASJ*, **52**, 153  
 Maughan, B. J., Jones, C., Forman, W., & Van Speybroeck, L. 2008, *ApJS*, **174**, 117  
 McDonald, M. 2011, *ApJL*, **742**, 35  
 McDonald, M., Veilleux, S., Rupke, D. S. N., & Mushotzky, R. 2010, *ApJ*, **721**, 1262  
 Melin, J.-B., Bartlett, J. G., & Delabrouille, J. 2006, *A&A*, **459**, 341  
 Mewe, R., Gronenschild, E. H. B. M., & van den Oord, G. H. J. 1985, *A&AS*, **62**, 197  
 Mortonson, M. J., & Hu, W. 2010, *PhRvD*, **81**, 067302  
 Mullis, C. R., Rosati, P., Lamer, G., et al. 2005, *ApJL*, **623**, 85  
 Muzzin, A., Wilson, G., Yee, H. K. C., et al. 2009, *ApJ*, **698**, 1934  
 Navarro, J. F., Frenk, C. S., & White, S. D. M. 1997, *ApJ*, **490**, 493  
 Papovich, C., Bassett, R., Lotz, J. M., et al. 2012, *ApJ*, **750**, 93  
 Papovich, C., Momcheva, I., Willmer, C. N. A., et al. 2010, *ApJ*, **716**, 1503  
 Pipino, A., & Matteucci, F. 2004, *MNRAS*, **347**, 968  
 Planck Collaboration, Ade, P. A. R., Aghanim, N., et al. 2011, *A&A*, **536**, A8  
 Popesso, P., Biviano, A., Romaniello, M., & Böhringer, H. 2007, *A&A*, **461**, 411  
 Reichardt, C. L., Stalder, B., Bleem, L. E., et al. 2012, arXiv:1203.5775  
 Rest, A., Stubbs, C., Becker, A. C., et al. 2005, *ApJ*, **634**, 1103  
 Rosati, P., Tozzi, P., Ettori, S., et al. 2004, *AJ*, **127**, 230  
 Rosati, P., Tozzi, P., Gobat, R., et al. 2009, *A&A*, **508**, 583  
 Rudnick, G. H., Tran, K.-V., Papovich, C., Momcheva, I., & Willmer, C. 2012, *ApJ*, **755**, 14  
 Samuele, R., McNamara, B. R., Vikhlinin, A., & Mullis, C. R. 2011, *ApJ*, **731**, 31  
 Santos, J. S., Rosati, P., Tozzi, P., et al. 2008, *A&A*, **483**, 35  
 Santos, J. S., Tozzi, P., & Rosati, P. 2011, *MSAIS*, **17**, 66  
 Saro, A., Bazin, G., Mohr, J., & Dolag, K. 2012, arXiv:1203.5708  
 Schlegel, D. J., Finkbeiner, D. P., & Davis, M. 1998, *ApJ*, **500**, 525  
 Skrutskie, M. F., Cutri, R. M., Stiening, R., et al. 2006, *AJ*, **131**, 1163  
 Snowden, S. L., Mushotzky, R. F., Kuntz, K. D., & Davis, D. S. 2008, *A&A*, **478**, 615  
 Snyder, G. F., Brodwin, M., Mancone, C. M., et al. 2012, *ApJ*, **756**, 114  
 Song, J., Zenteno, A., Stalder, B., et al. 2012, *ApJ*, **761**, 22  
 Stanford, S. A., Brodwin, M., Gonzalez, A. H., et al. 2012, *ApJ*, **753**, 164  
 Stanford, S. A., Eisenhardt, P. R., Brodwin, M., et al. 2005, *ApJL*, **634**, 129  
 Stanford, S. A., Romer, A. K., Sabirli, K., et al. 2006, *ApJL*, **646**, 13  
 Staniszewski, Z., Ade, P. A. R., Aird, K. A., et al. 2009, *ApJ*, **701**, 32  
 Stott, J. P., Collins, C. A., Sahl, M., et al. 2010, *ApJ*, **718**, 23  
 Sunyaev, R. A., & Zel'dovich, Y. B. 1972, *CoASP*, **4**, 173  
 Thomas, D., Maraston, C., Schawinski, K., Sarzi, M., & Silk, J. 2010, *MNRAS*, **404**, 1775  
 Tinker, J., Kravtsov, A. V., Klypin, A., et al. 2008, *ApJ*, **688**, 709  
 Tozzi, P., Rosati, P., Ettori, S., et al. 2003, *ApJ*, **593**, 705  
 Vanderlinde, K., Crawford, T. M., de Haan, T., et al. 2010, *ApJ*, **722**, 1180  
 Vikhlinin, A., Burenin, R., Forman, W. R., et al. 2007, in Heating versus Cooling in Galaxies and Clusters of Galaxies, ed. H. Böhringer, G. W. Pratt, A. Finoguenov, & P. Schuecker (Berlin: Springer), 48  
 Vikhlinin, A., Burenin, R. A., Ebeling, H., et al. 2009, *ApJ*, **692**, 1033  
 Waizmann, J.-C., Ettori, S., & Moscardini, L. 2012a, *MNRAS*, **420**, 1754  
 Waizmann, J.-C., Ettori, S., & Moscardini, L. 2012b, *MNRAS*, **422**, 3554  
 Whiley, I. M., Aragn-Salamanca, A., De Lucia, G., et al. 2008, *MNRAS*, **387**, 1253  
 Williamson, R., Benson, B. A., High, F. W., et al. 2011, *ApJ*, **738**, 139  
 Wilson, G., Muzzin, A., Yee, H. K. C., et al. 2009, *ApJ*, **698**, 1943